Research Paper

Int'l J. of Aeronautical & Space Sci. 11(2)145–153 (2010)
DOI:10.5139/IJASS.2010.11.2.145

IJASS
International Journal of Aeronautical and Space Sciences

Comprehensive Code Validation on Airloads and Aeroelastic Responses of the HART II Rotor

Young-Hyun You*, Jae-Sang Park and Sung-Nam Jung*****

Department of Aerospace Information Engineering, Konkuk University, Seoul 143-701, Korea

Do-Hyung Kim****

Rotor Department, Korea Aerospace Research Institute, Daejeon 305-333, Korea

Abstract

In this work, the comprehensive structural dynamics codes including DYMORE and CAMRAD II are used to validate the higher harmonic control aeroacoustic rotor test (HART) II data in descending flight condition. A total of 16 finite elements along with 17 aerodynamic panels are used for the CAMRAD II analysis; whereas, in the DYMORE analysis, 10 finite elements with 31 equally-spaced aerodynamic panels are utilized. To improve the prediction capability of the DYMORE analysis, the finite state dynamic inflow model is upgraded with a free vortex wake model comprised of near shed wake and trailed tip vortices. The predicted results on aerodynamic loads and blade motions are correlated with the HART II measurement data for the baseline, minimum noise and minimum vibration cases. It is found that an improvement of solution, especially for blade vortex interaction airloads, is achieved with the free wake method employed in the DYMORE analysis. Overall, fair to good correlation is achieved for the test cases considered in this study.

Key words: HART II, Comprehensive structural dynamics code, Blade vortex interaction airloads, Aeroelastic response

1. Introduction

The blade vortex interaction (BVI) is caused by interaction between the rotor blades and their trailed wakes. The BVI occurs mainly in low speed transition flight and causes significant noise and vibration problems. In order to improve the basic understanding for the formation of vortex wakes and the interactions leading to noise and vibration, an international cooperative program, HART II, was conducted in 2001 (Van der Wall, 2003), following the previous HART I (Yu et al., 2002). Particularly, the goals of the test were to measure the noise level, airloads, vortex wakes, and blade motions with and without higher harmonic pitch control (HHC) inputs.

After the test, a significant volume of research has been conducted for predicting BVI airloads and structural loads in reference to the measurement data constructed by the HART II program. The analyses range from low-order computational structural dynamics (CSD) methods (Lim et al., 2003; Lim and Van Der Wall, 2005; Van der Wall and Yin, 2007; Yeo and Johnson, 2005), hybrid methods (Min et al., 2009), and more sophisticated loose/tight CSD/computational fluid dynamics (CFD) coupled approaches (Lim, 2008; Potsdam et al., 2006; Yang et al., 2007). It is recognized that a CSD/CFD coupled analysis is desirable to effectively capture the BVI phenomena and to obtain accurate aeroelastic solutions. However, this requires heavy computing resources, even with state-of-the-art solution technologies. Computationally more efficient methodologies yielding reasonably accurate solutions are always needed for practical applications, especially at the preliminary design stage. In this regard, a lifting-line based CSD approach equipped with a free vortex

* Graduate Student
** Research Professor
*** Professor, Corresponding author, E-mail: snjung@konkuk.ac.kr, Tel: +82-2-450-3449, Fax: +82-2-444-6670
**** Senior Researcher

http://ijass.or.kr pISSN: 2093-274X eISSN: 2093-2480

wake model still deserves to be taken into consideration. The computed results from CSD analysis can be used as a datum at the stage of comparing and assessing the prediction capability of state-of-the-art analysis methods.

Recently, flexible multibody dynamics modeling techniques have attracted growing attention for use in rotorcraft applications. One of these techniques is DYMORE, which was developed by Bauchau (2007). DYMORE uses geometrically exact beam theory (Hodges, 1990) for nonlinear elastic beam model and the finite-state dynamic inflow model (Peters and He, 1995) for the aerodynamic model. The inflow model is a relatively simple estimate of the complex rotorcraft flow field; a more refined representation of aerodynamics is required for a more enhanced prediction (Liu, 2008; Min et al., 2009).

In order to improve the rotor wake modeling capability, Roget (2006) incorporated a time marching free vortex wake method developed by B-L (Bhagwat and Leishman, 2001) into DYMORE. This model has been applied to investigate the control authority of the active twist rotor and the active trailing-edge flap mechanism for a scaled rotor model. In the present work, the prediction capability of DYMORE with the B-L free vortex wake model is assessed for the evaluation of BVI airloads and blade motions of the HART II rotor with and without the higher harmonic control inputs. The comprehensive aeroelastic analysis code, CAMRAD II (Johnson, 1992), is also employed to cross-check the validity of blade modeling and to gain confidence about DYMORE predictions. Both the CSD predictions on airloads and structural responses of the rotor are correlated with the test data for the baseline (BL), minimum noise (MN), and minimum vibration (MV) cases.

2. HART II Test

The HART II test was conducted in an open-jet anechoic test chamber having an 8 m × 6 m cross-section in the German-Dutch wind tunnel (DNW). The rotor was operating under descent flight conditions with an advance ratio $\mu = 0.15$, a shaft tilt angle $\alpha_s = 5.3$ deg (4.5 deg after the wind tunnel wall correction), a hover tip Mach number $M = 0.6387$ and a thrust level $C_T = 0.0044$.

For the HART II rotor, 40% Mach-scaled models of the production BO-105 hingeless rotors were fabricated. The blade was dynamically scaled to match the natural frequencies of the first three flapping modes, the first two lag modes, and the first torsion mode of the full-scale versions. The chord length was increased by 10% to compensate for the Reynolds number error. The blades had a rectangular planform shape with -8 deg linear pretwist and 2.5 deg precone. The blades had a NACA23012 airfoil with a trailing-edge tab. The general properties of HART II blades are given in Table 1. Table 2 presents the forces and moments measured in the hub-fixed frame as well as the higher harmonic pitch inputs for the three test cases. It is noted that the roll and pitch moments are defined as positive when the advancing side goes down and when the nose-up motion is accompanied, respectively.

The cross-section of blades was composed of C-type spar, skin, and foam core. Both the skin and spar are made of fiberglass. The number 1 blade was designated as the reference blade and defined t he rotor azimuth. Each blade was instrumented with six strain gauges: three for flap, two for lead-lag, and one for torsion, while the reference and opposite blades (numbered one and three) were equipped with a root pitch sensor. The pitch link loads were also measured with a strain gauge attached to the pitch links.

The deflections of the HART II blades were measured optically by using the stereo pattern recognition (SPR) technique. Through this technique, 18 markers were distributed along the blade span and attached at both leading and trailing edges with an equal spacing starting from 22.8% radial location. The elastic blade motion was defined with respect to the rotor hub coordinate system. Both the flap and lead-lag motions were computed at the quarter chord line. The pitch angle θ_{SPR} is obtained using the vertical distance between the two markers (Δz) and their relative length along with a correction angle as:

$$\theta_{SPR} = \arctan\frac{\Delta z}{89\mathbf{mm}} + 1.65^{\circ} \quad (1)$$

The elastic twist ϕ is expressed in the following form by subtracting the pretwist angle θ_{tw}, the basic control, θ_0, θ_{1c}, θ_{1s}, and the 3/rev harmonic pitch inputs, θ_{3c}, θ_{3s}, from the measured pitch angle θ_{SPR}:

Table 1. General properties of HART II rotor blades

Properties	Values
Number of blades, N	4
Radius, R	2.0 m
Root cutout	0.44 m
Chord length, c	0.121 m
Solidity, σ	0.077
Blade mass	2.24 kg
Lock number	8.06
Nominal rotor speed, Ω	1,041 rpm

Table 2. Measured forces and moments, and higher harmonic control inputs for the test cases

	BL	MN	MV
Thrust, N	3300	3300	3290
Roll moment, N-m	20	30	20
Pitch moment, N-m	-20	-30	-30
θ_{3c}	0°	0.41°	-0.79°
θ_{3s}	0°	-0.70°	0.00°

BL: baseline, MN: minimum noise, MV: minimum vibration.

$$\phi = \theta_{SPR} - \theta_0 - \theta_{tw}(r - .75) - \theta_{1S}\sin\psi - \theta_{1C}\cos\psi - \theta_{3S}\sin 3\psi - \theta_{3C}\cos 3\psi \quad (2)$$

where r is the radial dis tance non-dimensioned by the length of the blade.

3. CSD Analysis

The comprehensive structural dynamics model used for the HART II validation is described in this section. A nonlinear flexible multi-body dynamics code DYMORE (Bauchau, 2007) as well as a comprehensive aeroelastic analysis code CAMRAD II (Johnson, 1992) are employed to obtain the aerodynamic loads acting on the blades and the corresponding structural responses of the rotor.

3.1 DYMORE with Free Wake Model

DYMORE is a nonlinear flexible multibody dynamics analysis system that includes rigid bodies, rigid/elastic joints, and elastic bodies such as beams, plates, and shells. It uses a geometrically exact beam theory (Hodges, 1990) for the elastic blade representation, a two-dimensional airfoil theory with an airfoil table look-up for the aerodynamic forces and moments, and Peters and He finite-state dynamic inflow model (Peters and He, 1995). This inflow model is constructed by applying the acceleration potential theory to a rotor aerodynamics problem with a skewed cylindrical wake. More specifically, the induced flow at the rotor disk is expanded in terms of modal functions. As a result, a three-dimensional, unsteady induced-flow aerodynamic model with a finite number of states is derived in the time domain. This model is an intermediate level of wake representation compared to the more complicated freewake methods.

The freewake analysis is based on a potential flow with the vorticity being concentrated on a finite number of vortex filaments. The motion of a point on a vortex filament is described by the motion of Lagrangian fluid markers as:

$$\frac{d\mathbf{r}(\psi,\zeta)}{dt} = \mathbf{V}\left(\mathbf{r}(\psi,\zeta)\right) \quad (3)$$

where r is the position vector of the point on the vortex filament and V is the local fluid velocity at the point r. In addition, ψ and ζ denote the blade azimuth angle and wake age, respectively. From Eq. (3), the vorticity transport equation is written in the following partial differential form:

$$\frac{d\mathbf{r}(\psi,\zeta)}{d\psi} + \frac{d\mathbf{r}(\psi,\zeta)}{d\zeta} = \frac{\mathbf{V}\left(\mathbf{r}(\psi,\zeta)\right)}{\Omega} \quad (4)$$

where Ω is the rotational speed. Eq. (4) dictates the governing equation for the free-vortex problem applied to the rotor wake. The left-hand-side of Eq. (4) is a one-dimensional wave equation. The complexity of the problem comes from the right-hand-side term, which is highly nonlinear. In order to solve Eq. (4), the domain (ψ, ζ) is discretized into finite steps of $\Delta\psi$ and $\Delta\zeta$. In addition, the derivatives of the left-hand-side in Eq. (4) are approximated by the finite difference scheme. The discretized equation is integrated by applying the time marching algorithm using predictor-corrector with the 2nd-order backward difference, as proposed by Bhagwat and Leishman (2001) and later modified by Roget (2006).

The trailed near wake is also taken into account to improve the accuracy of the solution. The near wake consists of a series of vortex filaments trailed behind the blades for a given angular distance. The trailed vortices comprise the near wakes, which are assumed to be planar with a fixed angular distance. The tip vortex that constitutes the freewake extends beyond the near wake with the strength equal to the maximum bound circulation along the blade. The strength of the blade bound vorticity is determined from the induced velocity at the control points.

The overall procedures to obtain the aerodynamic forces along the blades are described as follows: First, the aerodynamic lift is estimated by the two-dimensional strip theory using the inflow distribution obtained from the freewake model. Second, using the estimated lift, the angle of attack for the equivalent flat plate is determined. Third, the surface normal vector at the control point is adjusted to make it consistent with the equivalent flat plate angle of attack. Fourth, the blade bound circulations and the equivalent lifts are calculated. Finally, the effective angle of attack at each air station point is determined from a reverse table look-up procedure. This solution procedure allows for the circulation distribution on the blade to be consistent with the circulation released into the freewake.

3.2 CAMRAD II

CAMRAD II is a comprehensive aeromechanical analysis code that is characterized by multibody dynamics, nonlinear finite elements, and various levels of rotorcraft aerodynamics (Johnson, 1992). For the structural analysis, the blade motion consists of the sum of the rigid body motion and the elastic deformation. The rigid body motion describes the motion of one end of a beam element, and the elastic motion is measured relative to the rigid motion. Either Euler-Bernoulli or Timoshenko levels of approximations toward the beam representation is possible from the structural model depending upon the materials chosen for the blades. A quasi-static reduction of transverse shear variables is enforced to keep the number of degrees of freedom identical in both the beam approximations.

The aerodynamic model used in CAMRAD II is based on a lifting-line theory using steady two-dimensional airfoil characteristics and the vortex wake. Several different attached-flow unsteady aerodynamics along with various dynamic stall models are implemented in CAMRAD II. For the vortex wake model, the free wake geometry is used to compute the non-uniform induced inflow distribution around the rotor disk. The tip vortex formation is modeled using a rolled-up wake model that is constructed from the magnitude and position of peak bound circulation (Yeo and Johnson, 2005).

4. Results and Discussion

Both the DYMORE and CAMRAD II predictions of the HART II rotor are correlated with the wind tunnel measurement data. The test conditions considered for the HART II validation include the BL, MN, and MV cases. For both the MN and MV cases, 3/rev HHC inputs with different control phase angles are added to the pitch controls (Table 2).

Table 3. Trim analysis results for BL, MN, and MV cases

	BL		MN		MV	
	CAMRAD II	DYMORE	CAMRAD II	DYMORE	CAMRAD II	DYMORE
θ_0, deg	3.68	3.69	3.81	3.71	3.62	3.71
θ_{1c}, deg	1.16	2.06	1.33	2.05	1.16	2.10
θ_{1s}, deg	-1.40	-1.11	-1.37	-1.20	-1.44	-1.17

BL: baseline, MN: minimum noise, MV: minimum vibration.

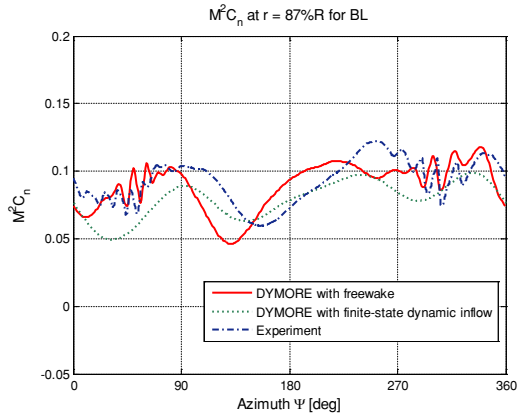

(a) M^2C_n

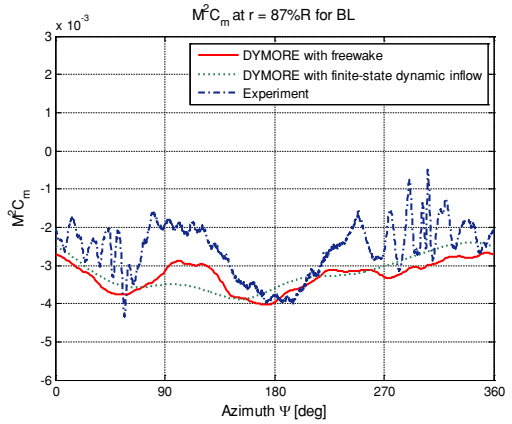

(b) M^2C_m

Fig. 1. Effect of inflow models on section normal forces and pitching moments at 87% station for the baseline (BL) case.

4.1 Aerodynamic Loads

The predicted airloads obtained for the three test cases under the descending flight condition are compared with the wind tunnel measurement records (Van der Wall, 2003). Both the predictions by DYMORE with B-L free wake model and CAMRAD II with roll-up wake model are correlated with the measured data. Table 3 summarizes the comparison of computed pitch control inputs obtained using CAMRAD II and DYMORE for each of the three test conditions. The pitch control inputs are obtained after the trim iterations are converged. The target values for the trim are given in Table 2.

Figure 1 shows the effect of different inflow models employed in the DYMORE analysis on the section normal force, M^2C_n, and pitching moments, M^2C_m, at 87% radial station for the BL case. The measurement data are also included for comparison purposes. The measured data shows strong BVIs in the advancing and retreating sides. It is seen that the predicted DYMORE results with a finite-state

DOI:10.5139/IJASS.2010.11.2.145

dynamic inflow model do not capture the BVI event along the azimuths. This is because the inflow model is based on simple harmonic functions and cannot describe high frequency BVI oscillations. Whereas, the free wake model improves the correlation drastically, especially at or near BVI events. It is notable that both the numbers and magnitudes of BVIs are captured quite nicely, but there is an apparent phase shift over the front disk area (ψ = 180 deg). No wake model is capable of capturing BVI oscillations in the section pitching moments since the lifting-line based model cannot describe the rapid movements of center of pressure during the BVI event.

Figure 2 shows the comparison of the section normal forces (a) and pitching moments (b) between the CAMRAD II and DYMORE predictions and measured data. The solid continuous line denotes the CAMRAD II results while the dashed line denotes the DYMORE results. The time step sizes of 15 deg and 1 deg are used for CAMRAD II and DYMORE analyses, respectively. Although mean airloads are reasonably predicted for both the CSD analyses, most of the BVI peaks are missed in the CAMRAD II predictions due to a large time step size used in the analysis. The CAMRAD II predictions show a slightly better correlation for the pitching moments as compared with the measurement data.

Figure 3 presents the comparison of normal forces, M^2C_n, and pitching moments, M^2C_m, obtained at 87% span location for the MN case. As compared with the BL case, a 3/rev variation of sectional lift is observed with the introduction of 3/rev HHC inputs. The number of measured BVI peaks becomes reduced significantly for the MN case, as compared with the absence of HHC control inputs. In general, DYMORE results with the free wake model show better correlation against the measured data than the CAMRAD II predictions, especially in advancing and retreating sides. However, a phase lead problem (about 20°) similar to the problem that occurred in the BL case is again observed in the DYMORE results. The peak-to-peak values of M^2C_n are reasonably captured with the CAMRAD II predictions. It is seen that there is a constant offset between the measured data and the CSD predictions for the estimation of M^2C_m.

The section normal forces and pitching moments at 87% radial location for the MV case are investigated next. Figure 4 shows the comparison results for the section normal forces and pitching moments. It is seen that the DYMORE analysis with free wake model shows a good correlation with measured data even though several BVI peaks in the first quadrant are missed and there remains a slight phase shift problem. The CAMRAD II predictions present better correlation in the phase angles.

The alternative way to look into BVI airloads is to find the gradient of the sectional lift with respect to the time, $d(M^2C_n)/d\psi$, because the highly impulsive and rapid fluctuating lifts during BVI events lead to sharp spikes in the gradient of sectional lifts. In other words, higher M^2C_n gradients mean stronger BVIs. Figure 5 shows a comparison of sectional lift gradients between DYMORE analysis with the free wake model and the measured data obtained for the three test cases. CAMRAD II results are not included because they do not capture BVI phenomenon at all. The time step size used for DYMORE analysis is 1 deg, whereas the

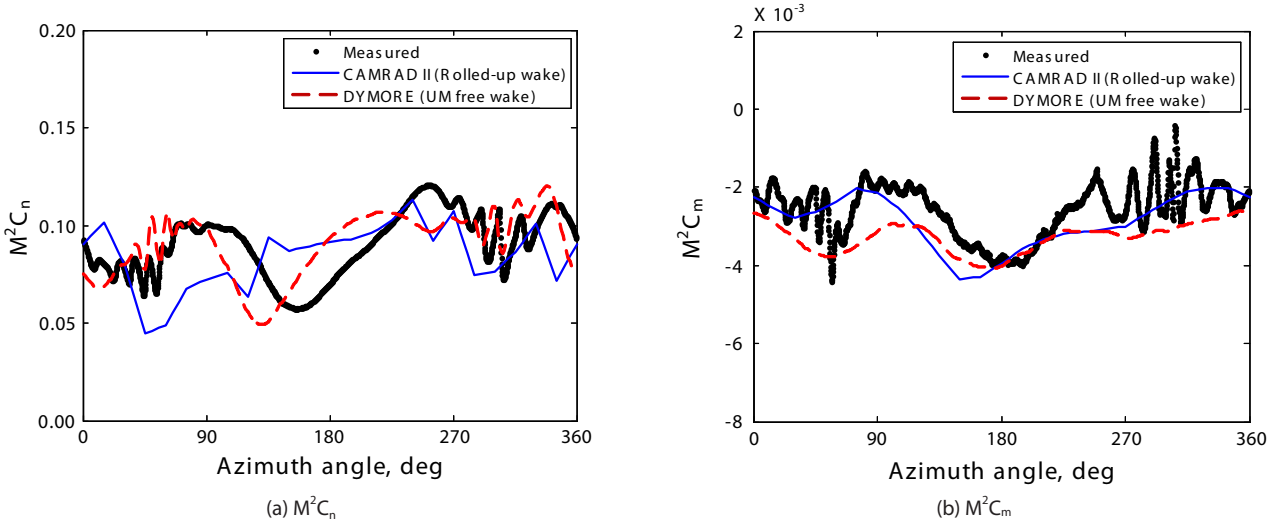

Fig. 2. Comparison of section normal forces and pitching moments at 87% station for the baseline case.

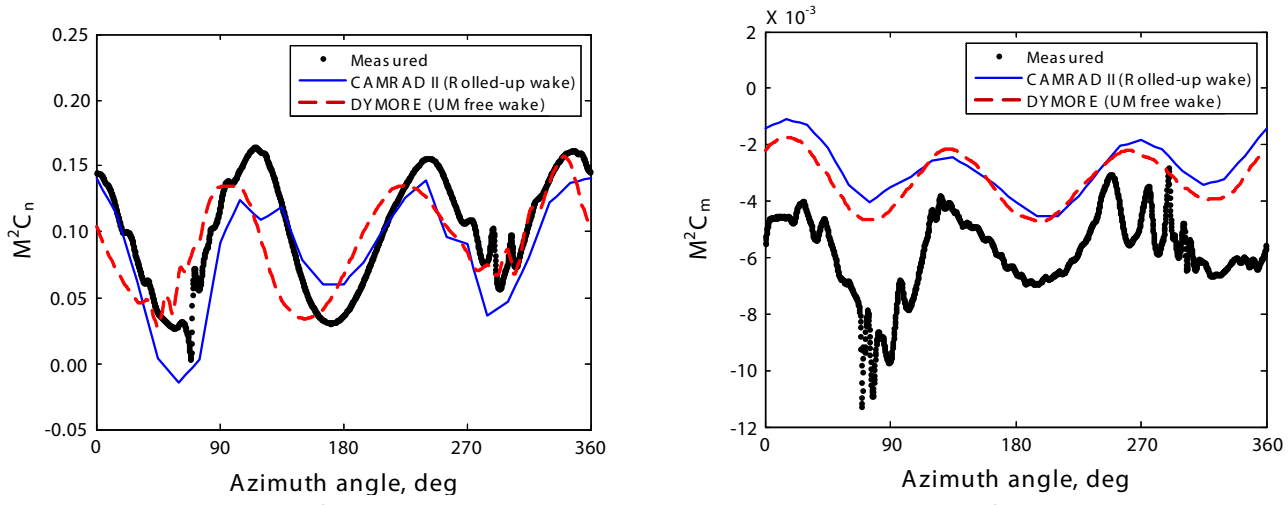

(a) M^2C_n (b) M^2C_m

Fig. 3. Comparison of section normal forces and pitching moments at 87% station for the minimum noise case.

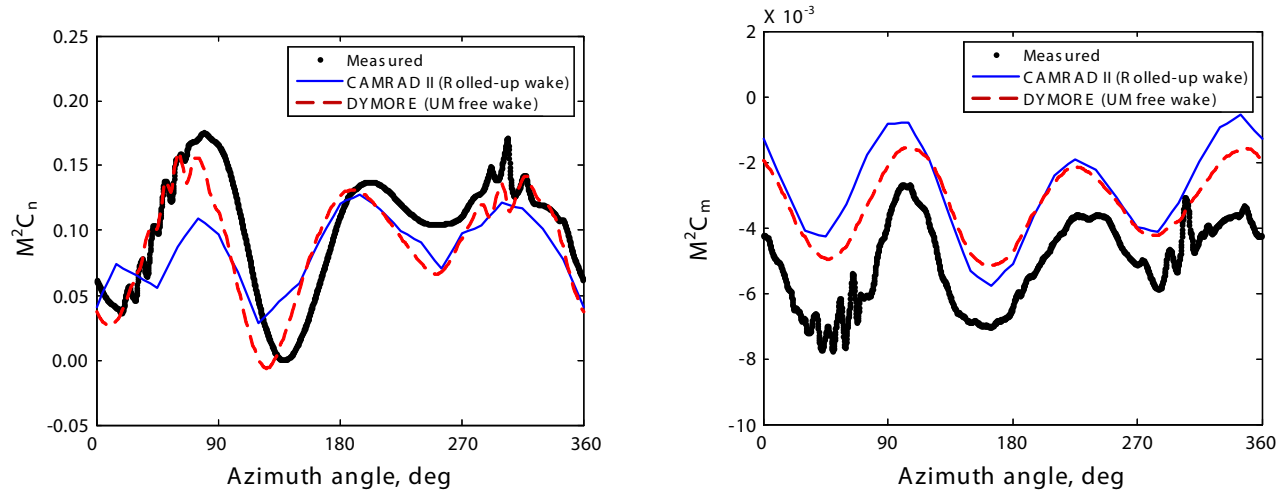

(a) M^2C_n (b) M^2C_m

Fig. 4. Comparison of section normal forces and pitching moments at 87% station for the minimum vibration case.

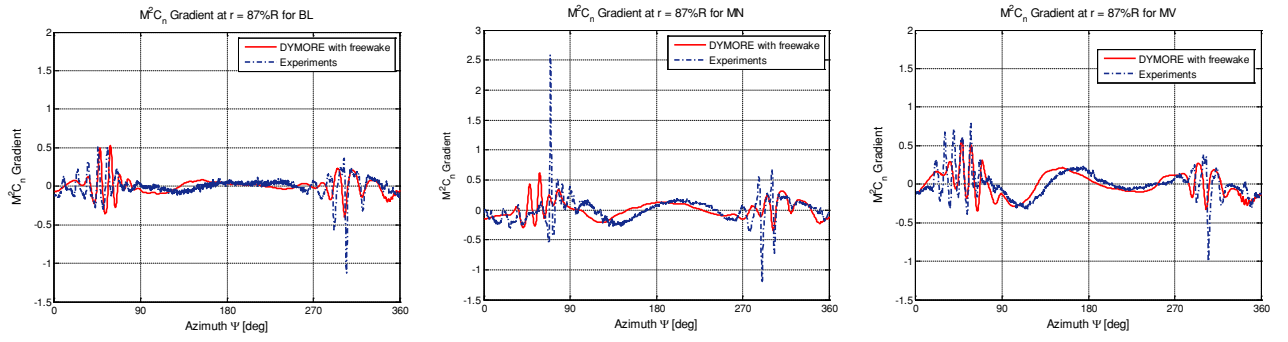

(a) BL case (b) MN case (c) MV case

Fig. 5. Comparison of section lift gradient at 87% radial station for the three cases. BL: baseline, MN: minimum noise, MV: minimum vibration.

DOI:10.5139/IJASS.2010.11.2.145

experimental data has 0.176 deg. In order to compensate for the inconsistency, DYMORE results are interpolated using the cubic spline technique leading a time step of 0.25 deg. As is denoted in Fig. 5, the correlation with experimental data is generally within the range of good to fair for most cases. The BVI peaks in the advancing side are reasonably captured with the present analysis for both the BL and MV cases, but the predicted peaks of the MN case are much less impulsive compared to the measurement data. In addition, the predictions show under-estimation of BVI peaks at around 300 deg azimuth angles for all the cases. More refined representation of aerodynamic loads seems required to enhance the correlation.

4.2 Blade Structural Response

Figure 6 shows the comparison of time variation of flap, lead-lag, and torsion deformation at the blade tip between the measured data and the predicted results computed by CAMRAD II and DYMORE for the BL case. The blade deflections are measured at 24 azimuth positions in increments of 15°. For simplicity, only the measured deflections of the reference blade (No. 1 blade) are presented, even though the experimental data show significant blade-to-blade dissimilarities (Lim, 2008; Van der Wall and Yin, 2007). The sign convention for each of the blade deflections is defined as positive when the blade undergoes flap-up, lag-back, and nose-up deformation, respectively. The flap deflections are obtained by removing the precone angles from the vertical displacements, while the elastic twist deformation is obtained by subtracting the pitch control inputs and pretwist angles from the total geometric pitch angle, as given in Eq. (2).

As is seen in Fig. 6, the correlation is generally good for the flap deflections, while the correlation is fair to poor for the elastic torsion and lead-lag deflections, respectively. It is indicated that there are constant offsets amounting to approximately 1/3 chord length between the measured and predicted lead-lag deflections. This trend has also been observed in previous investigations (Lim, 2008; Lim et al., 2003) and similar results are obtained in the present predictions. The DYMORE results are in better agreement with the measured flap deflections than the CAMRAD II predictions, but the peak-to-peak magnitudes of lead-lag deflections by DYMORE are larger than those with other methods. The 2/rev characteristics of the measured elastic twist deformation are captured well with the DYMORE, however the mean values are correlated better with the CAMRAD II.

Figures 7 and 8 show the comparison of tip deflections in flap, lead-lag, and torsion for the MN and MV cases, respectively. As is expected from the rotor with 3/rev HHC inputs, a clear 3/rev response is noticed for both the flap and elastic twist deformation. The correlations between the predictions and test results are generally good for flap and torsion deflections, but the lead-lag deflections show constant offsets between predicted results and measured data. For the flap response, the CAMRAD II predictions show better correlation in the MN case; however, better correlation is noticed with DYMORE in the MV case, as compared with measurement data. It is indicated that the HHC inputs do not affect much on the lead-lag response. The lead-lag deflections obtained for both the MN and MV case show only a marginal difference as compared with the BL case. Except the lead-lag deflections, the analysis results slightly under-predict the peak-to-peak response compared to the measured values.

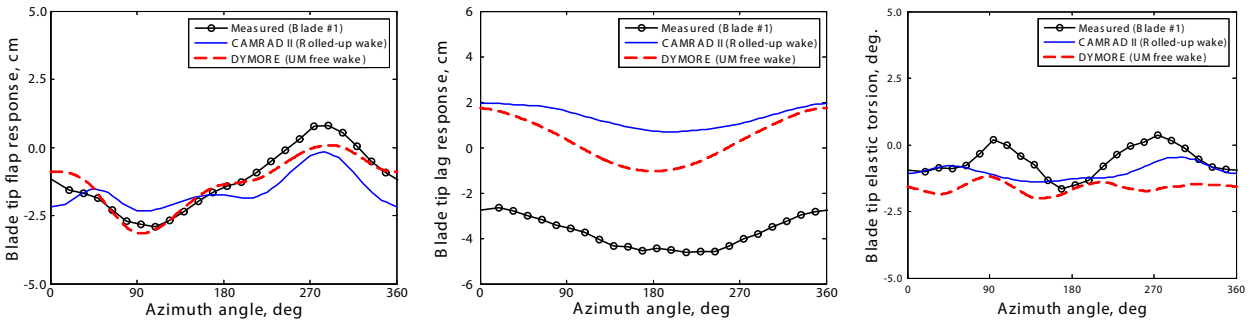

(a) Flap deflection (b) Lead-lag deflection (c) Elastic twist deformation

Fig. 6. Comparison of tip displacements for the baseline case.

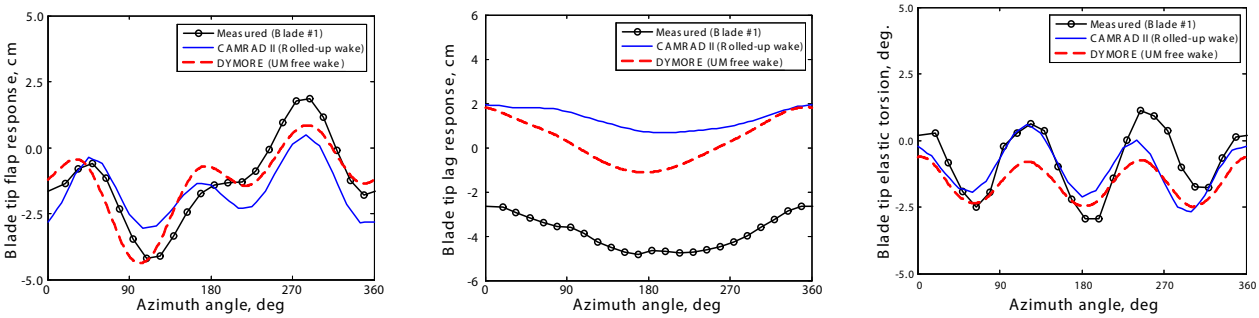

(a) Flap deflection (b) Lead-lag deflection (c) Elastic twist deformation

Fig. 7. Comparison of tip displacements for the minimum noise case.

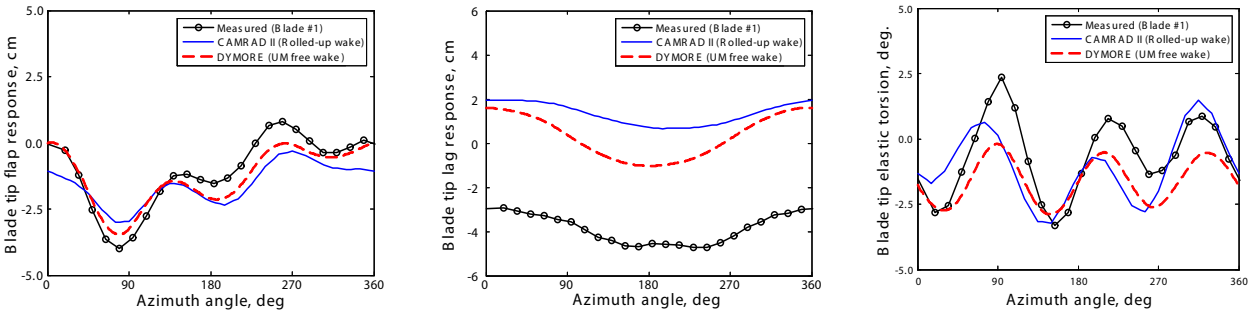

(a) Flap deflection (b) Lead-lag deflection (c) Elastic twist deformation

Fig. 8. Comparison of tip displacements for the minimum vibration case.

5. Conclusions

In this work, the prediction capability of CSD codes including DYMORE and CAMRAD II has been demonstrated for the HART II rotor with and without higher harmonic control inputs. The test conditions considered include the BL, MN, and MV cases. A B-L free vortex wake model comprised of near shed wake and trailed tip vortices is implemented in the DYMORE analysis. It is found that the free wake model improves significantly on the BVI airloads prediction at both advancing and retreating sides compared with the finite-state dynamic inflow model. However, both CSD codes are able to capture the BVI event for section pitching moments. The gradient of airloads demonstrates reasonable correlation, but result in less impulsive responses as compared with the measured data. With regard to the blade motions, fair to good correlation is obtained with both the CSD predictions. A further study is required to enhance this correlation. It is believed that the current study provides a useful database for a comprehensive comparison, and this investigation will become a stepping stone toward more refined aeroelastic analysis such as the CFD/CSD coupled methodology.

Acknowledgements

This work was supported by National Research Foundation (NRF) through a grant provided by the Korean Ministry of Education, Science & Technology (MEST) in 2009 (No. K20601000001). This study has been supported by Korea Aerospace Research Institute (KARI) under the KHP Dual-Use Component Development Program funded by the MKE. The authors express sincere thanks to Dr. Berend Van der Wall at DLR and all participating members of the HART II test team for their invaluable efforts and the test data.

References

Bauchau, O. A. (2007). DYMORE User's Manual. Savannah, GA: Georgia Institute of Technology.

Bhagwat, M. J. and Leishman, J. G. (2001). Stability, consistency and convergence of time-marching free-vortex rotor wake algorithms. *Journal of the American Helicopter Society*, 46, 59-71.

Hodges, D. H. (1990). A mixed variational formulation

based on exact intrinsic equations for dynamics of moving beams. *International Journal of Solids and Structures*, 26, 1253-1273.

Johnson, W. (1992). *CAMRAD II, Comprehensive Analytical Model of Rotorcraft Aerodynamics and Dynamics*. Palo Alto, CA: Johnson Aeronautics.

Lim, J. W. (2008). An assessment of rotor dynamics correlation for descending flight using CFD/CSD coupled analysis. *64th Annual AHS Forum*, Montreal. pp. 239-260.

Lim, J. W., C, T., Yu, Y. H., Burley, C., Brooks, T., Boyd, D., Van der Wall, B. G., Schneider, O., Richard, H., Raffel, M., Beaumier, P., Bailly, J., Delrieux, Y., Pengel, K., and Mercker, E. (2003). HART II: prediction of blade-vortex interaction loading. *29th European Rotorcraft Forum*, *Friedrichshafen*, Germany.

Lim, J. W. and Van Der Wall, B. G. (2005). Investigation of the effect of a multiple trailer wake model for descending flights. *61st Annual AHS Forum*, Grapevine, TX. pp. 1063-1081.

Liu, H. (2008). *Interfacing Comprehensive Rotorcraft Analysis with Advanced Aeromechanics and Vortex Wake Models*. PhD Thesis, Georgia Institute of Technology.

Min, B. Y., Sankar, L., Prasad, J. V. R., and Schrage, D. (2009). A physics-based investigation of gurney flaps for rotor vibration reduction. *65th Annual AHS Forum*, Grapevine, TX. pp. 139-149.

Peters, D. A. and He, C. J. (1995). Finite state induced flow models part II: three-dimensional rotor disk. *Journal of Aircraft*, 32, 323-333.

Potsdam, M., Yeo, H., and Johnson, W. (2006). Rotor airloads prediction using loose aerodynamic/structural coupling. *Journal of Aircraft*, 43, 732-742.

Roget, B. (2006). Simulation of active twist and active flap control on a model-scale helicopter rotor. *24th AIAA Applied Aerodynamics Conference*, San Francisco, CA. pp. 1681-1696.

Van der Wall, B. G. (2003). *2nd HHC Aeroacoustic Rotor Test (HART II)-Part I: Test Documentation-Institute Report IB 111-2003/31*. Braunschweig, Germany: German Aerospace Center (DLR).

Van der Wall, B. G. and Yin, J. (2007). DLR's S4 rotor code validation with HART II data: the baseline case. *International Forum on Multidisciplinary Technology*, Seoul, Korea.

Yang, C., Inada, Y., and Aoyama, T. (2007). BVI noise prediction using HART II motion data. *International Forum on Multidisciplinary Technology*, Seoul, Korea.

Yeo, H. and Johnson, W. (2005). Assessment of comprehensive analysis calculation of airloads on helicopter rotors. *Journal of Aircraft*, 42, 1218-1228.

Yu, Y. H., Tung, C., Van der Wall, B. G., Pausder, H. J., Burley, C., Brooks, T., Beaumier, P., Delriuex, Y., Mercker, E., and Pengel, K. (2002). The HART-II test: rotor wakes and aeroacoustics with higher-harmonic pitch control (HHC) inputs. *58th Annual AHS Forum*, Montreal, Canada.